



# Validation of Integrated Multisatellite Retrievals for GPM (IMERG) by using gauge-based analysis products of daily precipitation over East Asia

Juwon Lee<sup>1</sup> · Eun-Hee Lee<sup>1</sup> · Kyung-Hee Seol<sup>1</sup>

Received: 15 January 2017 / Accepted: 10 December 2018 / Published online: 4 January 2019  
© Springer-Verlag GmbH Austria, part of Springer Nature 2019

## Abstract

This paper documents the qualities of satellite-based daily precipitation products from Integrated Multisatellite Retrievals for Global Precipitation Measurement (IMERG) over East Asia. Evaluations for a year from June 2014 to May 2015 are performed using gauge-based precipitation analysis from the Climate Prediction Center (CPC) and Global Precipitation Climatology Centre (GPCC) and other satellite-based high-resolution precipitation products, such as Tropical Rainfall Measuring Mission Multisatellite Precipitation Analysis (TMPA) and the Climate Prediction Center Morphing Method (CMORPH), are also compared. The results indicate that satellite products effectively capture seasonal variations in precipitation over East Asian land regions from spring to fall although overall underestimation with relatively low correlations is observed during winter. The verification of daily detection for various thresholds indicates that IMERG and TMPA products exhibit similarly higher correspondence to CPC while CMORPH exhibits persistent underestimation for all thresholds and especially in winter. The IMERG and TMPA products tend to underestimate with decreasing thresholds and overestimate with increasing thresholds against CPC, although this tendency is significantly reduced when validated with GPCC. Nevertheless, the overall performance of IMERG and TMPA are comparable and IMERG shows reliable performance in daily precipitation for all seasons, indicating less bias and higher skill scores against those of gauge-based precipitations. The assessment study suggests the validity of the IMERG product for daily precipitation over East Asia, and this exhibits the potential for use as reference precipitation data to validate numerical weather prediction models.

## 1 Introduction

Precipitation is extremely important to human life and the planetary water cycle, and its accurate estimation and prediction are crucial to weather forecasters and climate scientists and to various application areas, such as hydrology, agriculture, and industry, and a wide range of decision makers. Among the available global precipitation measurement data, rain gauge observation represents the most direct method to measure the amount of surface rainfall. However, given the limitation of spatial coverage of the gauge observation over several parts of the world,

satellite-based precipitation products (i.e., Huffman et al. 2007, 2010; Joyce et al. 2004; Sorooshian et al. 2000; Behrangi et al. 2009; Aonashi et al. 2009) have been widely used in research and applications globally. Simultaneously, verification of satellite precipitation products has become an integral part of the development and refinement of the retrieval techniques. A number of intercomparison studies have explored global satellite precipitation products including the Global Precipitation Climatology Project (GPCP), Algorithm Intercomparison Program (Ebert et al. 1996; Arkin and Xie 1994; Ebert and Manton 1998), and National Aeronautics and Space Administration (NASA) Precipitation Intercomparison Projects (Dodge and Goodman 1994; Barrett et al. 1994; Smith et al. 1998; Adler et al. 2001).

Recently, merged high-resolution satellite precipitation products (HRPPs) are available [(e.g., Precipitation Estimation from Remotely Sensed Information using Artificial Neural Networks (PERSIANN); Sorooshian

✉ Eun-Hee Lee  
eh.lee@kiaps.org

<sup>1</sup> Korea Institute of Atmospheric Prediction Systems, 4F, 35 Boramae-ro-5-gil, Dongjak-gu, Seoul 07071, South Korea

et al. 2000), Climate Prediction Center Morphing Method (CMORPH; Joyce et al. 2004), Tropical Rainfall Measuring Mission (TRMM) Multisatellite Precipitation Analysis (TMPA; Huffman et al. 2007)]. Among them, TMPA is one of the most popular products due to its reliability and relatively long data record (starting in 1997). A new integrated satellite precipitation product, namely Integrated MultisatellitE Retrievals for Global Precipitation Measurement (IMERG), was constructed based on the success of the widely used TMPA products and was released through the Global Precipitation Measurement (GPM) mission (Hou et al. 2014; Huffman et al. 2015a, b, c). IMERG considers the global and regional error characteristics in TMPA estimates as a benchmark, but it integrates advantages of other multisatellite precipitation products including CMORPH and PERSIANN. Therefore, researchers are naturally motivated to evaluate the new product with other HRPPs or observation prior to its active use to estimate global precipitation although preliminary comparisons between the IMERG Final Run and TMPA monthly products for June 2014 were performed by Huffman et al. (2015c). Liu (2016) reported the reliability of the IMERG Final Run monthly product compared with TMPA 3B43, and the results indicated that the differences varied with surface types (ocean or land) and precipitation rates in summer and winter. However, the validity of the IMERG precipitation product for not only seasonal precipitation but also daily precipitation detection needs to be evaluated further such that it can be potentially used as precipitation reference data to validate NWP models. The study by Prakash et al. (2016) documented that the IMERG exhibits significant improvements relative to the TMPA in terms of capturing heavy rainfall over India during the southwest monsoon season, and this is an example of an investigation involving the IMERG product. Kim et al. (2017) and Lee and Lee (2018) also addressed the potential of IMERG estimates for near-real-time precipitation or reference precipitations to evaluate weather forecasting models based on their validation results relative to the gauge network over Korea.

In this study, we compare the characteristics of the IMERG precipitation product with those of other HRPPs, TMPA, and CMORPH over the East Asian domain (ranging from 20 to 50° N and 70–145° E) and evaluate daily precipitation estimates with gauge-based precipitation data. Data descriptions and methodology are given in “[Data and methodology](#)” section. “[Analysis of rainfall distributions](#)” section provides the results of the geographic comparison among the precipitation dataset, and “[Analysis of conditional detection](#)” section focuses on the validation of daily precipitation detection by HRPPs with gauge-based reference data over the land region. The summary and conclusions is given in “[Summary and conclusion](#)” section.

## 2 Data and methodology

We compare the performance of three satellite precipitation products: IMERG, TMPA, and CMORPH. The study domain covers East Asia ranging from 20 to 50° N and 70–145° E (shown in Fig. 1) and encompasses the Taklamakan Desert and Tibet Plateau in the western boundary and Japan in the eastern boundary. The study duration corresponds to a year from June 2014 to May 2015. In order to evaluate the performance of precipitation products, Climate Prediction Center (CPC) gauge-based analysis of daily precipitation is used as a reference.

### 1. Satellite precipitation products

#### a. IMERG

IMERG (Huffman et al. 2015a, b, c) Version 3 data was used. From June 2014 to May 2015, 30-min global precipitation data collected given in 0.1° resolution, over 60° S–60° N, was analyzed. The IMERG precipitation product is produced by an integrated algorithm of several multisatellite retrievals, and it includes precipitation estimates from passive microwave (PMW) sensors on board various precipitation-relevant satellites in the GPM constellation and zenith-angle-corrected, intercalibrated infrared (IR) fields merged from several geostationary (GEO) satellites (Janowiak et al. 2001). The PMW sources used in the IMERG include most TMPA sources, but GPM sensors are more often used, which suggests significant changes in PMW precipitation estimates from TMPA (Liu 2016). The PMW-IR precipitation combined estimates are bias-corrected by the monthly Global Precipitation Climatology Centre (GPCC) gauge analysis precipitation products (Schneider et al. 2011). Among the three half-hourly products (Early, Late, and Final Run), the Final Run products were used in this study.

#### b. TMPA

TMPA 3B42-V7, the post-real-time research-grade product available over 50° S–50° N, was used in this study. The horizontal resolution is 0.25° × 0.25°, and 3-hourly data was processed. The TMPA algorithm (Huffman et al. 2007, 2010) consists of multiple precipitation estimates from various PMW sources, including the TRMM Microwave Imager (TMI), Special Sensor Microwave Imager (SSM/I), Advanced Microwave Scanning Radiometer (AMSR), Advanced Microwave Sounding Unit B (AMSU-B)/Microwave Humidity Sounder (MHS), and GEO IR. The PMW-IR combined estimates are re-scaled against monthly accumulated rain gauge analysis from the GPCC (Schneider et al. 2011) over land.

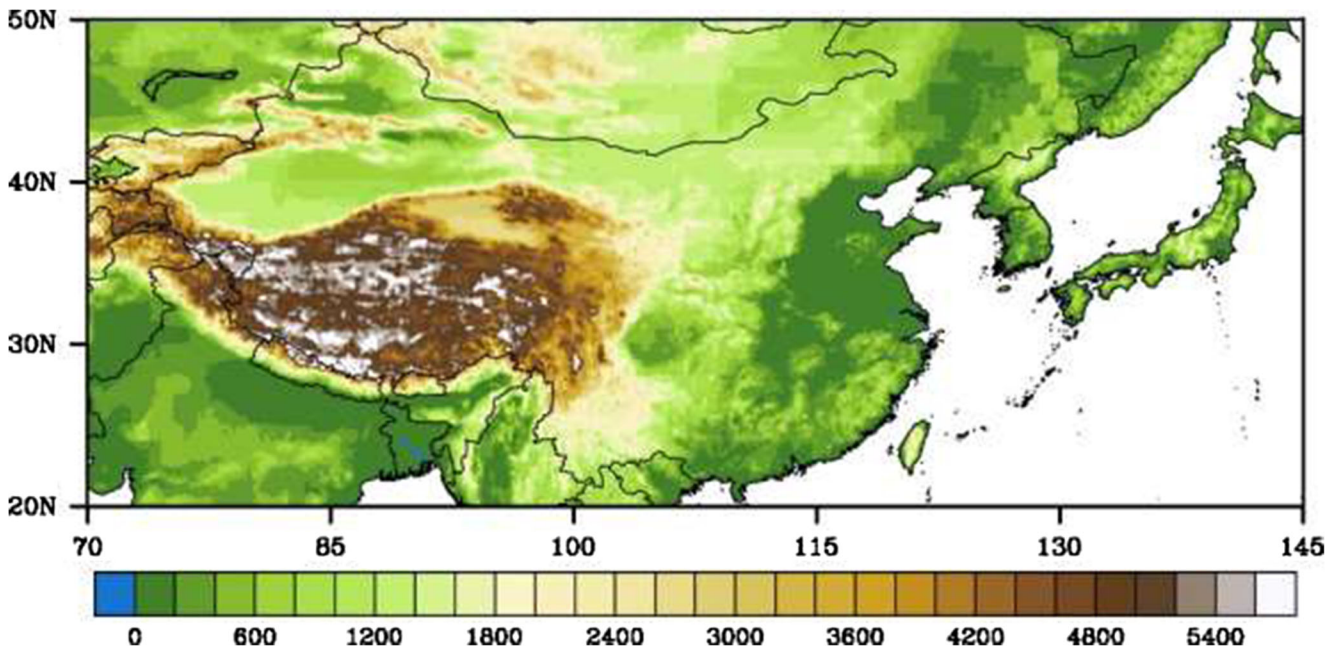


**Fig. 1** Study domain with topography (m) shown from ETOPO 5-min gridded elevation data from the National Centers for Environmental Information, National Ocean and Atmospheric Administration

### c. CMORPH

The CMORPH product, providing half-hourly data on a grid with a spacing of 8 km covering 60° S–60° N, was also compared. The National Oceanic and Atmospheric Administration (NOAA)/CPC developed CMORPH to provide precipitation information with high spatial and temporal resolution (Joyce et al. 2004; Joyce and Xie 2011). The CMORPH combines rainfall estimates from multiple PMW sensors, including the AMSU-B, SSM/I, TRMM, TMI, and AMSR for Earth Observing System (AMSR-E) but calibrates against TMI values. Therefore, to fill the time and space gap due to insufficient global coverage by microwave measurement, the algorithm uses cloud motion vectors derived from spatial lag correlations of successive GEO satellite IR images. The shape and intensity of the rainfall patterns are then morphed through linear interpolation by using weights obtained from the forward advection and backward advection of rainfall features.

### 2. Surface reference dataset

NOAA CPC unified gauge-based analysis of global daily precipitation, which is constructed over the global land areas, was used as reference precipitation data for validation. Gauge reports from over 30,000 stations are collected from multiple sources, including the Global Telecommunications System (GTS), Cooperative Observer Network (COOP), and other national and international agencies. Quality control is performed through comparisons with historical records and independent information from measurements at nearby stations,

concurrent radar/satellite observations, as well as numerical model forecasts. Quality controlled station reports are then interpolated to create analyzed fields of daily precipitation considering orographic effects (Xie et al. 2007; Chen et al. 2008). The daily analysis is constructed on a 0.125° lat/lon grid over all global land areas and released on a 0.5° lat/lon grid over the global domain for a period from 1979 to the present. The CPC gauge-based data is only available over land areas, but the gauge density over East Asia is generally very good (Xie et al. 2007), so it can be regarded “truth.” The “real-time version” which uses 17,000 stations was used in this study.

Furthermore, GPCC-daily precipitation data with a resolution of 1° × 1° was also used for comparison purpose that involves understanding the characteristics of precipitation products of the IMERG and TMPA since GPCC-monthly is used for the bias correction of IMERG and TMPA as mentioned previously. The GPCC collects rain gauge data from across the globe from the national meteorological agencies among approximately 150 countries and 31 regional suppliers, and it receives daily surface synoptic observations and monthly climate messages from the World Meteorological Organization Global Telecommunication System. Therefore, the GPCC data product is the most commonly used product and covers the period from 1901 to the present (Sun et al. 2018).

### 3. Data pre-processing

In order to perform the intercomparison analysis, the IMERG, TMPA, and CMORPH products were compared

against gauge-based daily precipitation data from the CPC gauge-based precipitation analysis. The IMERG, TMPA, CMORPH, and CPC data have different horizontal resolutions corresponding to  $0.1^\circ \times 0.1^\circ$ ,  $0.25^\circ \times 0.25^\circ$ ,  $8 \times 8 \text{ km}^2$ , and  $0.5^\circ \times 0.5^\circ$ , respectively. Therefore, all data were re-gridded to match the CPC grid with simple box averaging, and daily precipitation products were subsequently composited by considering the time resolution of each dataset based on the Universal Time Coordinate (UTC).

### 3 Analysis of rainfall distributions

Figure 2 compares the seasonal rainfall characteristics of the three satellite precipitation products and the CPC observation for 1 year from June 2014 to May 2015. It is shown that all the precipitation products effectively capture the horizontal distributions of mean precipitation with relevant seasonal variation corresponding to Asian monsoon season. Agreement among the products is observed across the land regions while larger discrepancy is observed over the East China Sea. Over land, the IMERG and TMPA products present significantly similar distributions over all seasons, thereby indicating high correlations with the CPC gauge data. The slight observed difference is that TMPA exhibits higher precipitation over the South Asian region in summer. Conversely, the CMORPH underestimates rainfall when compared with other precipitation products throughout all seasons. The discrepancy of the CMORPH is more conspicuous over the monsoon rainfall region in Southeast Asia in summer. The differences among products are more noticeable over the ocean where the IMERG estimates lower precipitation amounts when compared with the other two satellite-based products.

The higher correspondence of IMERG and TMPA to the gauge-based CPC precipitation is attributed to their inclusion of bias correction by gauge precipitation using GPCC-monthly. Figure 2 also compares the GPCC seasonal precipitation with a resolution of  $1^\circ$ . In addition to the resolution difference, two gauge-based data show very high agreement with the exception of over the northern Indochina peninsula and mountainous regions of the Himalaya where the GPCC shows overall higher precipitation distributions. The discrepancy is potentially caused by the differences in the number of observation stations used in the two gauge-based data processes as noted by Sun et al. (2018).

In order to compare the accuracy of the satellite-derived precipitation products, the spatial bias ratio and correlation are analyzed relative to gauge-based precipitations. In the analysis, a daily precipitation comparison is conducted only for the case of the observation detection counted by the minimum value for the precipitation detection corresponding to  $0.1 \text{ mm day}^{-1}$ . Figure 3a shows the seasonal mean distribution of the daily bias ratio of satellite precipitation against the CPC. The most noticeable characteristic in the seasonal bias distributions is that all precipitation

products show clear underestimation for winter precipitation. Besides the winter season, the IMERG and TMPA have similar bias ratio distributions, showing overall slight overestimation with the exception of the northwestern part of the analysis domain. On the other hand, the CMORPH product shows bias distribution patterns that significantly differ from those of the other two satellite-based products. For example, in summer and fall, the CMORPH exhibits underestimation over the extensive heavy rainfall regions including South Asia and Southeastern Asia, Southern China, Korea, and Japan. While missing points are only observed in winter for IMERG and TMPA precipitation, they are more frequently observed in the CMORPH product. Thus, discontinuous bias patterns of CMORPH precipitation are observed over the dry regions, such as the Tibetan Plateau in spring and fall, and also over the overall northern boundary of the domains including Korea and Japan in winter.

The same evaluation is performed but against GPCC gauge precipitation and the results are given in Fig. 3b but after processed to the GPCC's resolution. The results reveal that the overall overestimated bias ratio of IMERG and TMPA is reduced when examined relative to GPCC, thereby implying, as expected, that the quality of the two products highly affected the bias correction with rain gauge observation. It also shows that the abnormal overestimation found around the Himalayan mountainous regions shown in Fig. 3a is significantly reduced in the comparison with the GPCC. With the exception of the aforementioned differences and resolutions, the bias features of satellite precipitation products relative to two gauge precipitation are identical.

The spatial distribution of the seasonal mean correlation coefficient of daily precipitation is given in Fig. 4. When the three products are verified against CPC precipitation (Fig. 4a), they show relatively high correlation coefficient over the heavy rainfall regions from South Asia to Northeastern China while they have poor correlations over the dry regions, such as Northwestern China and higher latitude regions of Northern China. In winter, all products reveal relatively poor performance with the exception of South Asia and Southern China regions. A comparison of the precipitation products indicates that the IMERG exhibits higher correlations when compared with the two other precipitation products throughout all seasons while the CMORPH shows relatively low correlations, thereby indicating especially low correlations close to zero over wide regions in the winter. This suggests the possibility that CMORPH techniques exhibit incomplete estimation over cold areas. When they are verified relative to GPCC  $1^\circ$  data, a slight improvement is observed for IMERG and TMPA and especially for the summer season (Fig. 4b), but the spatial discrepancy is not that noticeable when compared to those shown in the bias ratio.

Figure 5 shows the scatterplots for the daily precipitation obtained from the CPC gauge-based data and the three

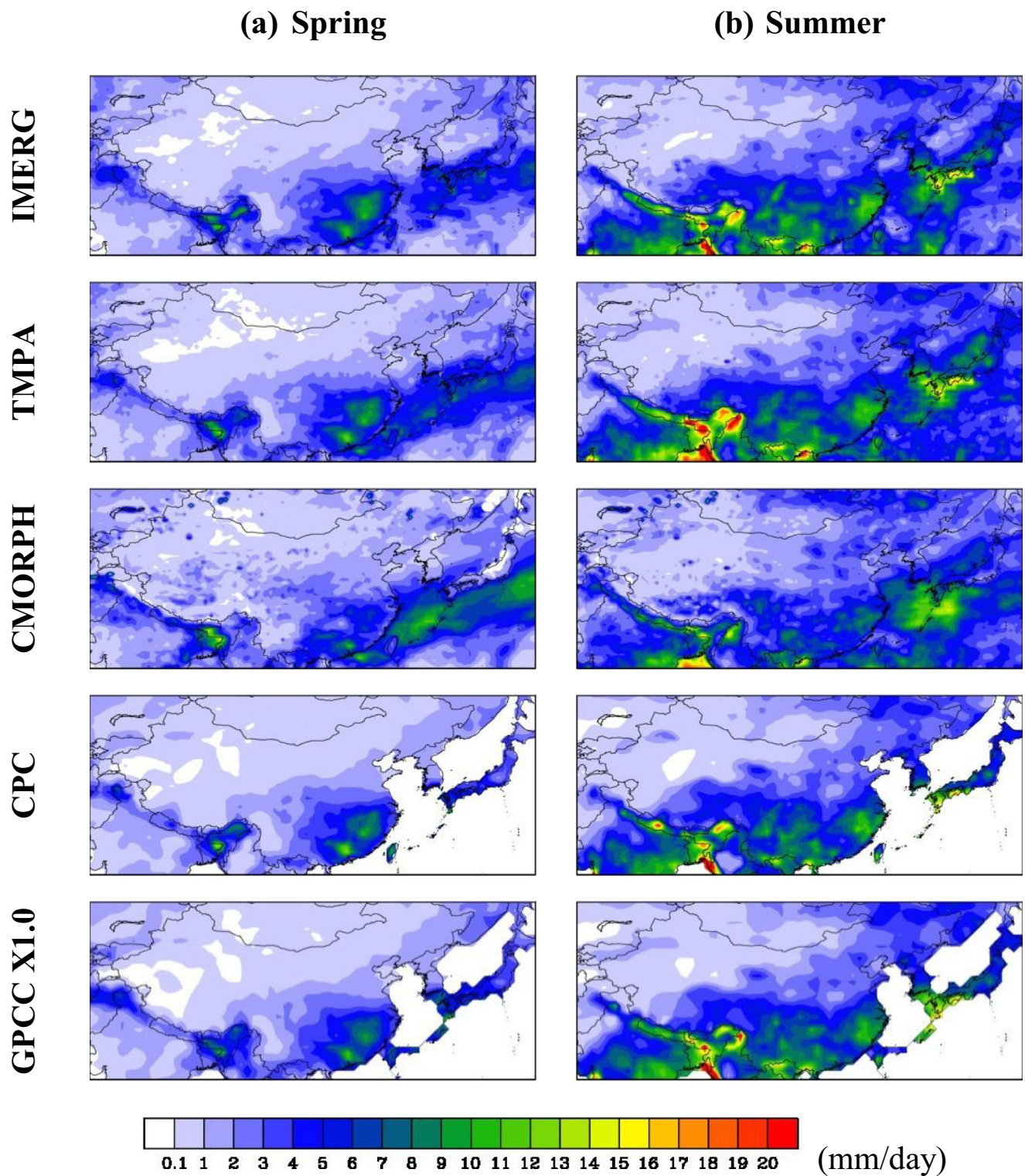


Fig. 2 Spatial distributions of seasonal mean precipitation from three HRPPs of IMERG, TMPA, and CMORPH processed with  $0.5^\circ$  resolution and comparison with CPC unified gauged-based daily precipitation ( $0.5^\circ \times 0.5^\circ$ ). GPCC ( $1^\circ \times 1^\circ$ ) gauge-based precipitation is also given for comparison

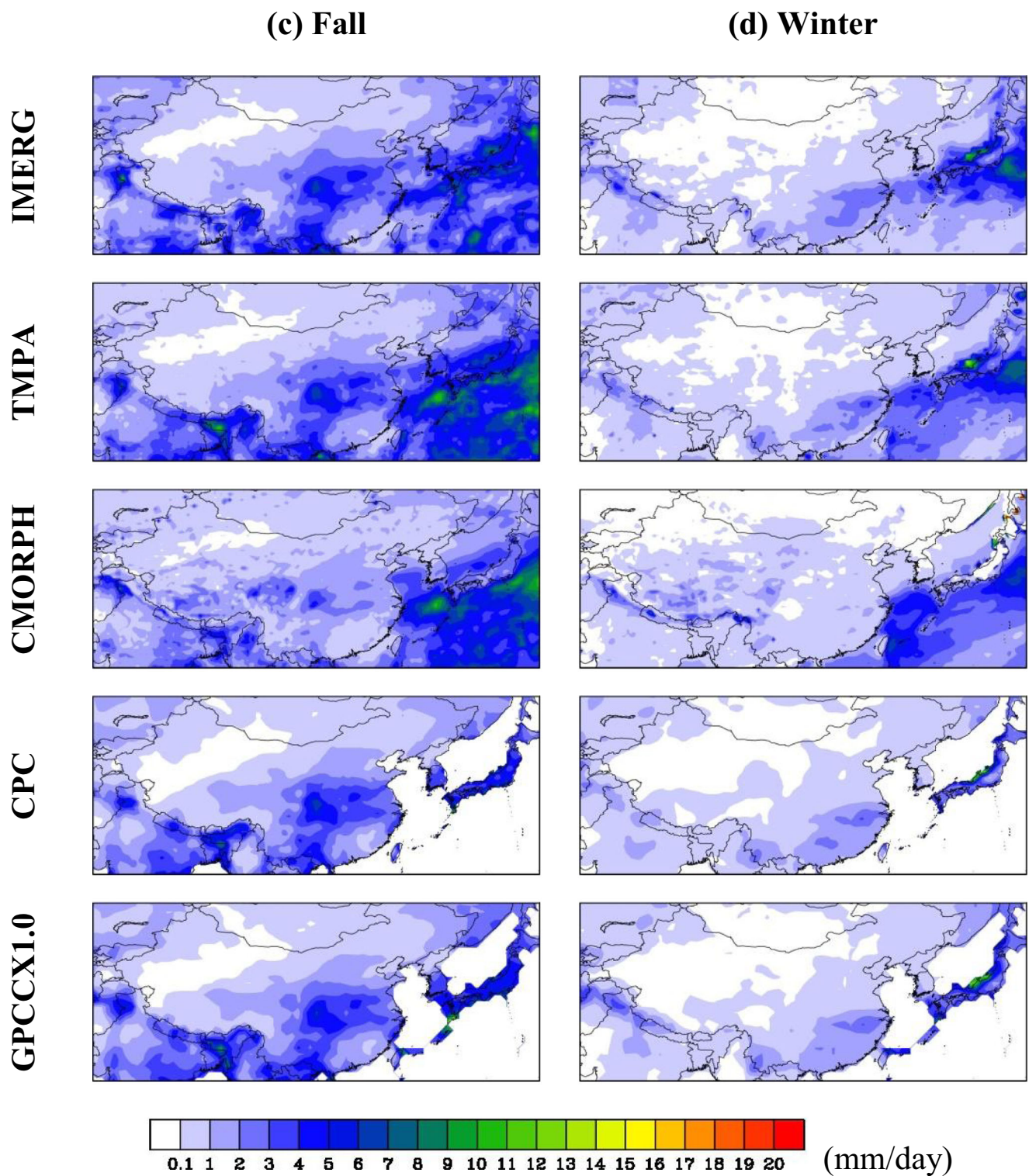
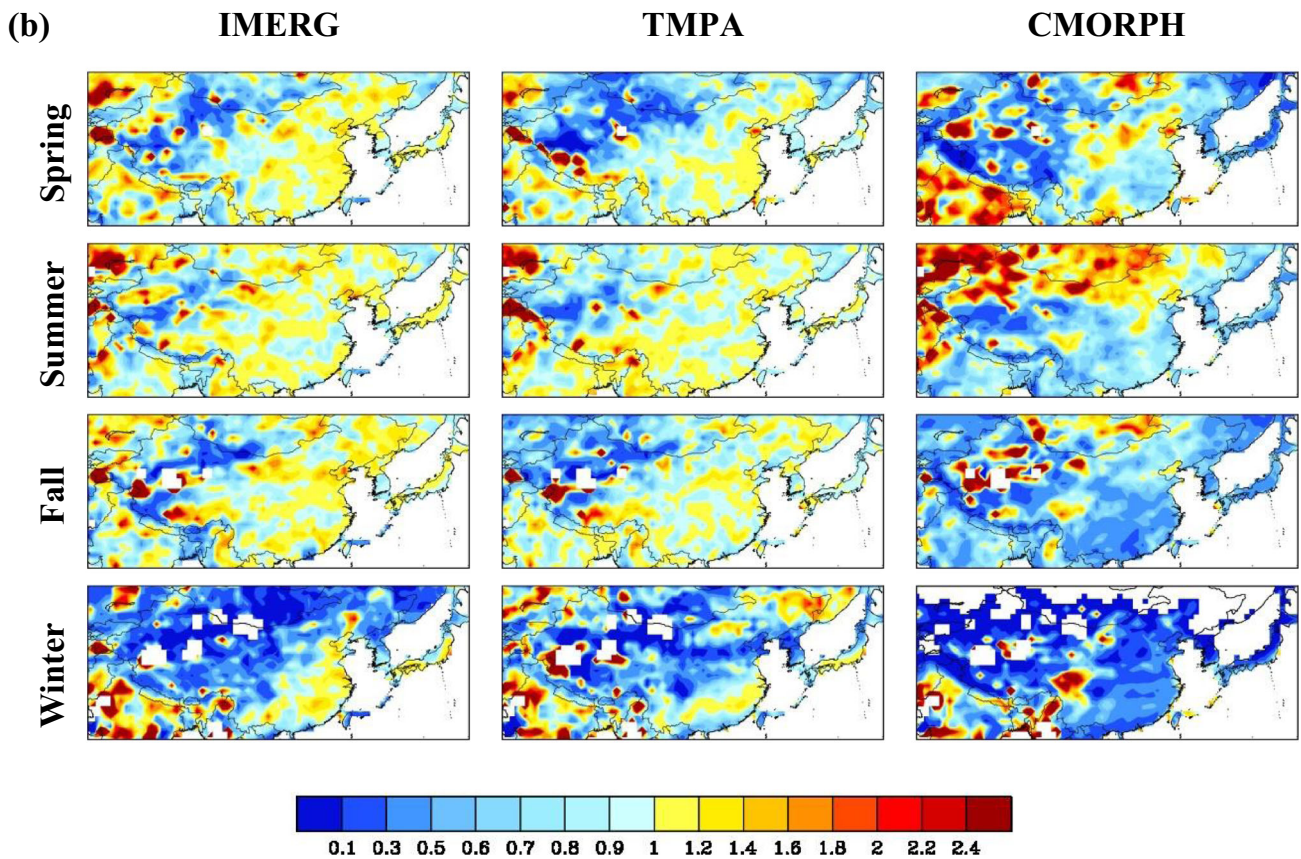
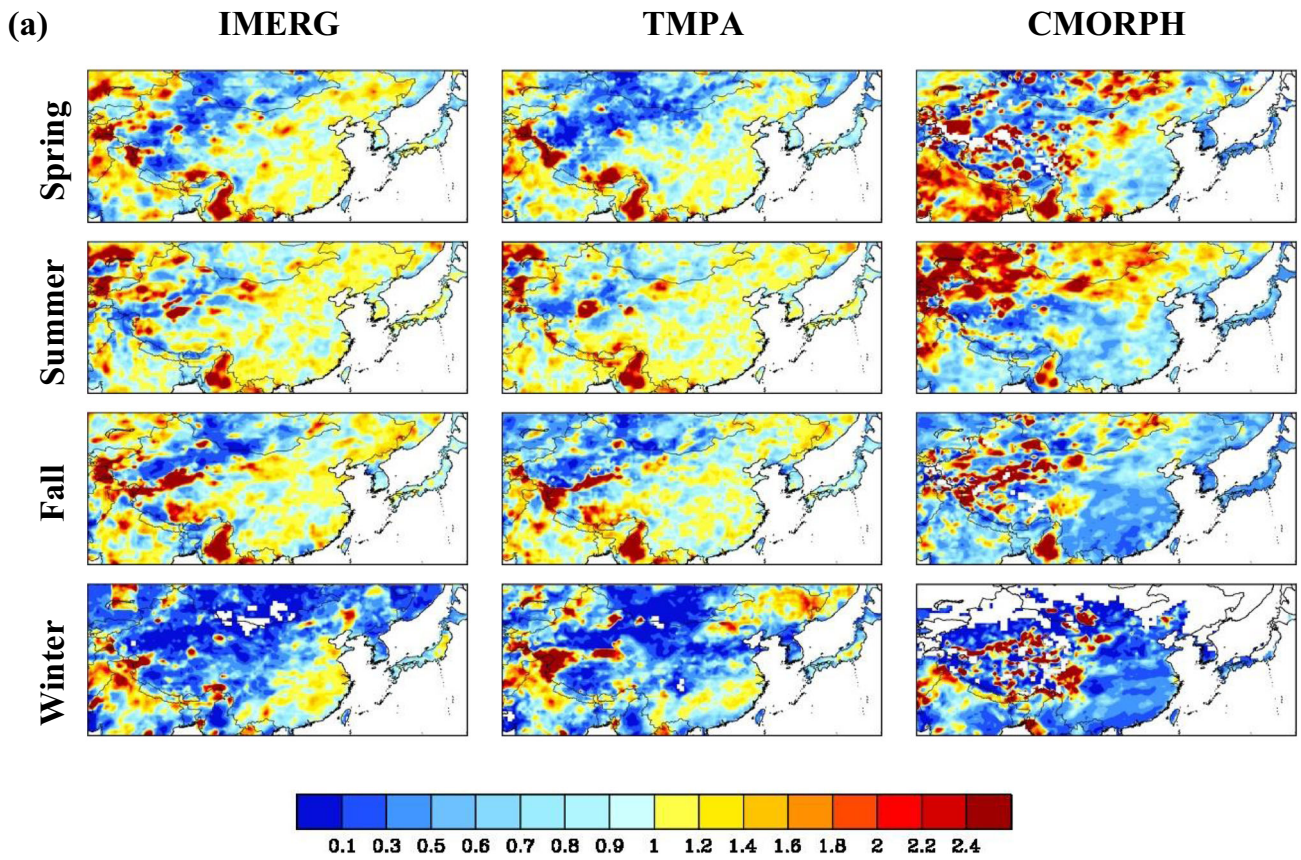
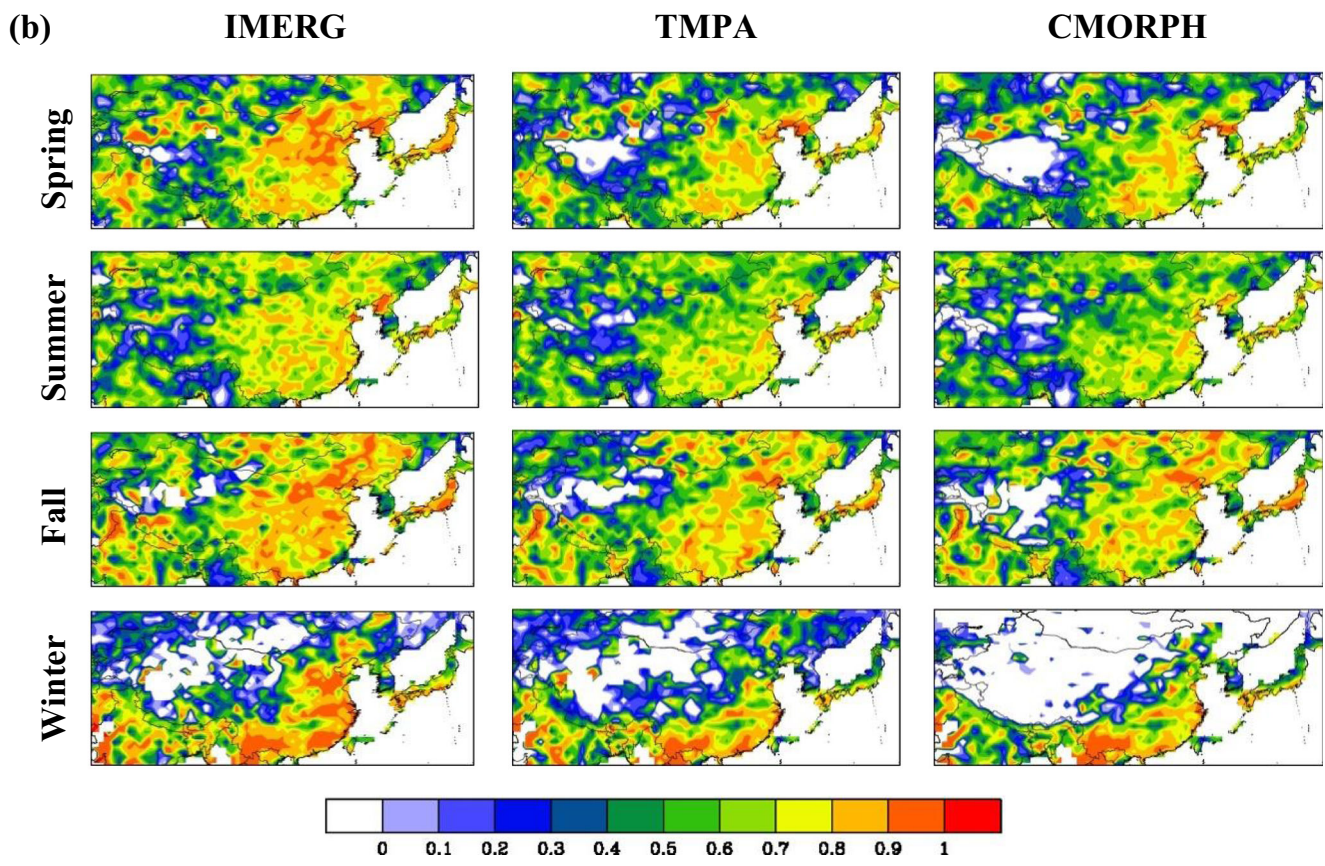
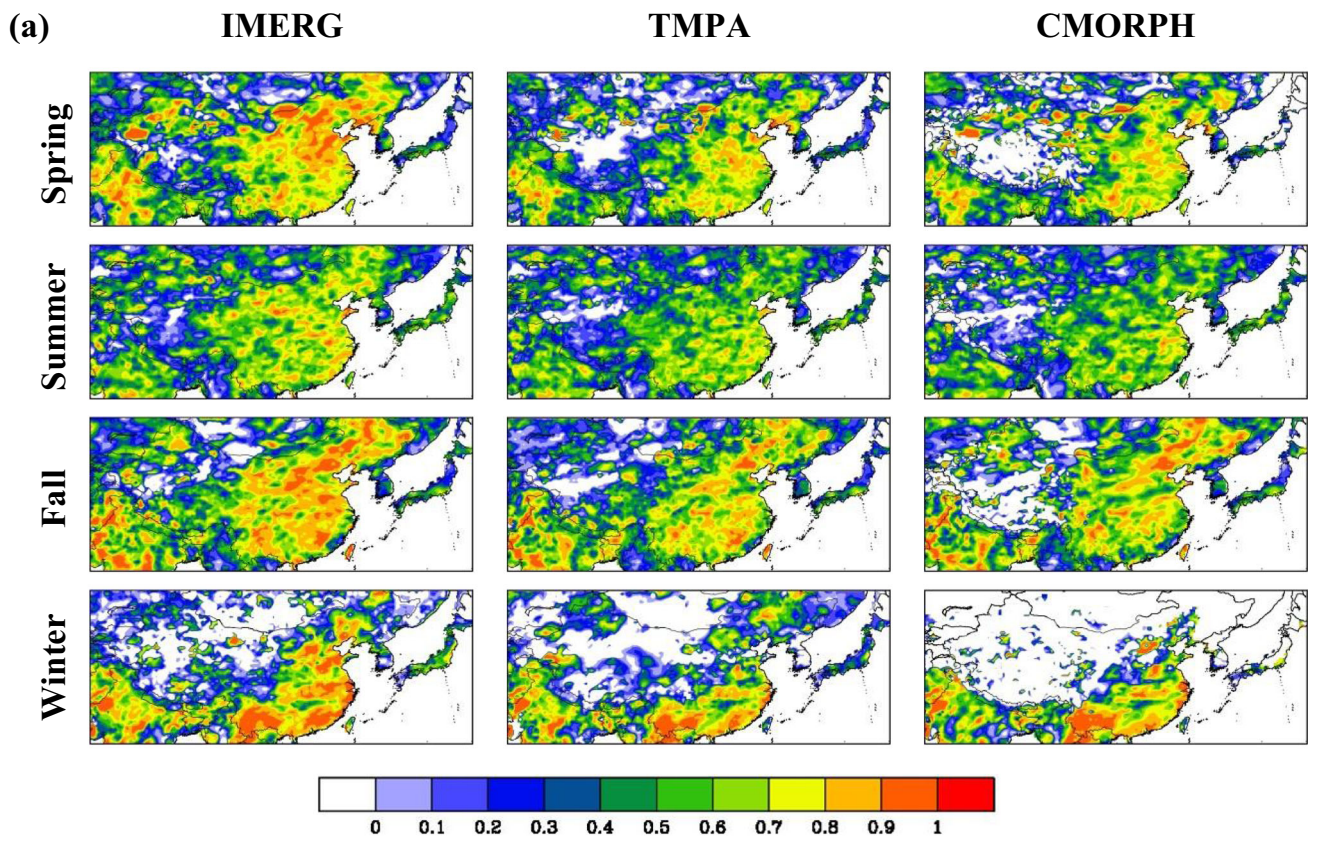


Fig. 2 (continued)

HRPPs. It is found that the overall seasonal correlations of the three products are in a similar range (around 0.7) from spring to fall, and the discrepancy among products is more noticeable

**Fig. 3** Spatial distributions of the seasonal mean bias ratio of IMERG, TMPA, and CMORPH daily precipitation against (a) CPC-daily ( $0.5^\circ \times 0.5^\circ$ ) and (b) GPCC-daily ( $1^\circ \times 1^\circ$ ). Evaluations of satellite precipitation are performed with the same resolution as the individual reference data







**Fig. 4** Spatial distributions of the seasonal mean correlation coefficient of IMERG, TMPA, and CMORPH daily precipitation against **a** CPC-daily ( $0.5^\circ \times 0.5^\circ$ ) and **b** GPCC-daily ( $1^\circ \times 1^\circ$ ). Evaluations of satellite precipitation are performed with the same resolution as the individual reference data

in the correlations of the winter season, showing less than 0.6 in TMPA ( $R = 0.53$ ) and CMORPH ( $R = 0.41$ ). In the comparison between IMERG and TMPA, IMERG provides consistently high correlations (exceeding 0.7) over all seasons.

#### 4 Analysis of conditional detection

The accuracy of daily precipitation products was quantitatively verified by assessing their conditional detection skill, which was measured by various skill scores based on a  $2 \times 2$  contingency table method. As shown in Fig. 6, the  $2 \times 2$  contingency table lists the total number of hits (a), false alarms (b), misses (c), and correct negatives (d), from which categorical statistics are derived to evaluate the accuracy of estimated rain occurrence. Performance measures used in the analysis include frequency Bias index (Bias), equitable threat score (ETS), symmetric extreme dependency score (SEDS), probability of detection (POD), success ratio (SR), and critical success index (CSI) (see Fig. 6 for descriptions of each). By considering the seasonal mean precipitation distribution analysis in the “Analysis of rainfall distributions” section, we selected four precipitation thresholds of corresponding to 1, 5, 15, and 30 mm day<sup>-1</sup>.

Figure 7 presents the seasonal Bias index of the IMERG, TMPA, and CMORPH products against CPC gauge data for daily precipitation thresholds of 1, 5, 15, and 30 mm day<sup>-1</sup>. It appears that both IMERG and TMPA tend to underestimate with decreasing in the precipitation thresholds and overestimate with increasing in the precipitation thresholds by presenting similar performance characteristics of underestimation for the thresholds of 5 mm day<sup>-1</sup> and overestimation for heavy rainfall thresholds exceeding 15 mm day<sup>-1</sup>. On the other hand, the CMORPH shows consistent underestimation for all threshold ranges and for all seasons (bias less than 1), and this appears more significant in winter with a low bias of approximately 0.3.

In the comparison of IMERG and TMPA, bias for all seasons reveals that the IMERG estimation is larger than TMPA estimation by presenting overall larger bias values, except heavier rainfall in winter. Thus, IMERG shows quite unbiased performance, especially for the 5-mm day<sup>-1</sup> threshold, by showing a bias quite close to 1, but it yields significantly overestimated detection for precipitation thresholds above 15 mm day<sup>-1</sup>. With the exception of winter, TMPA estimates more unbiased detection for threshold exceeding 15 mm day<sup>-1</sup>, thereby suggesting that the TMPA product

has better performance capabilities in detecting heavy precipitation events in East Asia.

Figure 8 shows the seasonal ETSs of the IMERG, TMPA, and CMORPH products verified against CPC gauge data for daily precipitation thresholds corresponding to 1, 5, 15, and 30 mm day<sup>-1</sup>. It is found that all HRPPs show the highest performance in detecting precipitation events in summer and the lowest performance in detecting winter events. Among them, the smallest ETS is found in CMORPH products for all seasons, and its performance degradation is more noticeable in winter. It is potentially related to the overall underestimation of CMORPH products shown in Fig. 7. As shown in the figure, TMPA and IMERG products present similar performance characteristics in terms of ETS. However, IMERG exhibits better performance in the light precipitation range corresponding to 5 mm day<sup>-1</sup> while TMPA shows better performance in the heavy precipitation range of 30 mm day<sup>-1</sup>. For example, IMERG has the highest ETS up to 0.27 for the threshold less than 5 mm day<sup>-1</sup> in summer, and TMPA shows the highest ETS around 0.2 for the heavy rainfall threshold higher than 15 mm day<sup>-1</sup> in summer and fall.

Since all HRPPs have degraded performance in winter (i.e., ETSs for the three HRPPs are the lowest (below 0.2)), it needs to be examined with other skill measures for precipitation detection. As documented by Hogan et al. (2009), ETS tends to be unbiased only with large data samples, and this can affect the results analyzed for the dry season. Therefore, the skill of detecting precipitation events is measured by an additional skill score, namely the SEDS. The SEDS is introduced as an alternative measure to verify the performance of numerical weather prediction models for rare events, taking advantage of the non-vanishing property of the score when the event probability tends to zero (Hogan et al. 2009). As shown in Fig. 6, the SEDS is subsequently defined as:

$$\text{SEDS} = (\log[(a + b)/n] + \log[(a + c)/n]) / (\log(a/n) - 1) \quad (1)$$

where  $n$  stands for the total number of data points ( $n = a + b + c + d$ ). The score varies from 0 (worst value) to 1 (best value).

Figure 9 presents the seasonal SEDSs of the IMERG, TMPA, and CMORPH products verified against CPC gauge data for the daily precipitation thresholds of 1, 5, 15, and 30 mm day<sup>-1</sup>. A comparison with the ETS scores in Fig. 8 shows that all HRPPs reveal more consistent performance in terms of SEDSs among seasons. Among three HRPPs, IMERG and TMPA are more comparable. The IMERG exhibits the highest SEDS for all threshold values in spring and winter (Fig. 9a, d) and TMPA exhibits a high SEDS of approximately 0.6 (summer) or above 0.6 (fall) for heavy rainfall thresholds in summer and fall (Fig. 9b, c). In short, the findings in terms of the performance comparison are consistent with those described in Fig. 8.

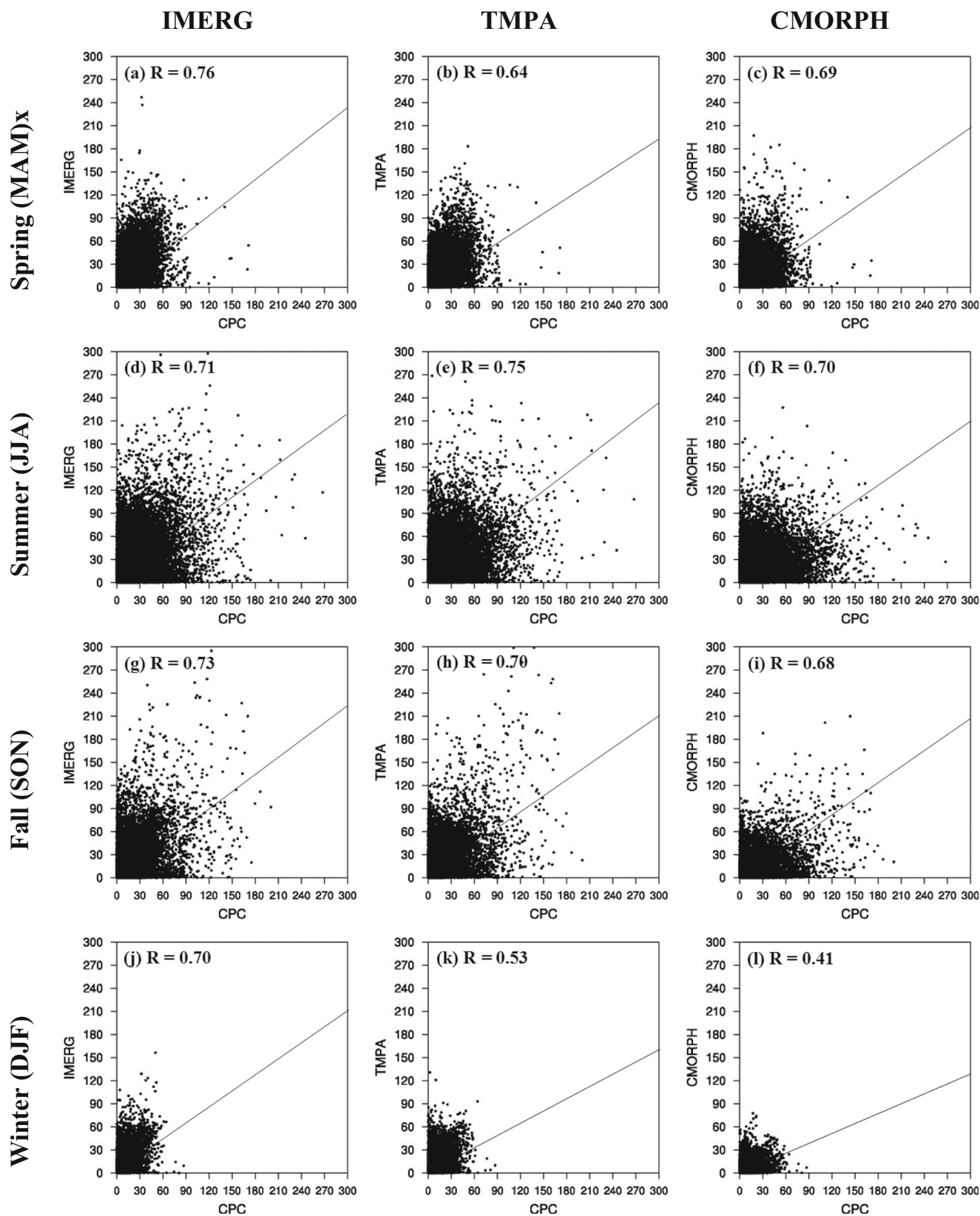


**Fig. 5** Scatterplots of the daily precipitation obtained from IMERG, TMPA, and CMORPH vs. CPC gauge-based data. Solid line denotes a least square regression line, and correlation coefficients ( $R$ ) between satellite precipitation products and CPC gauge data are given on the top left of each plot

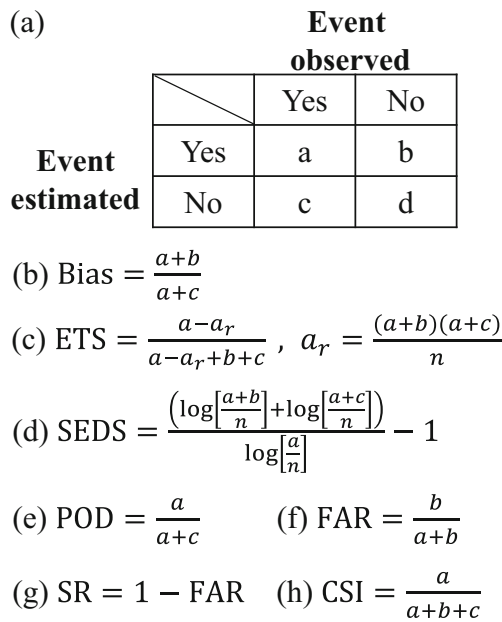
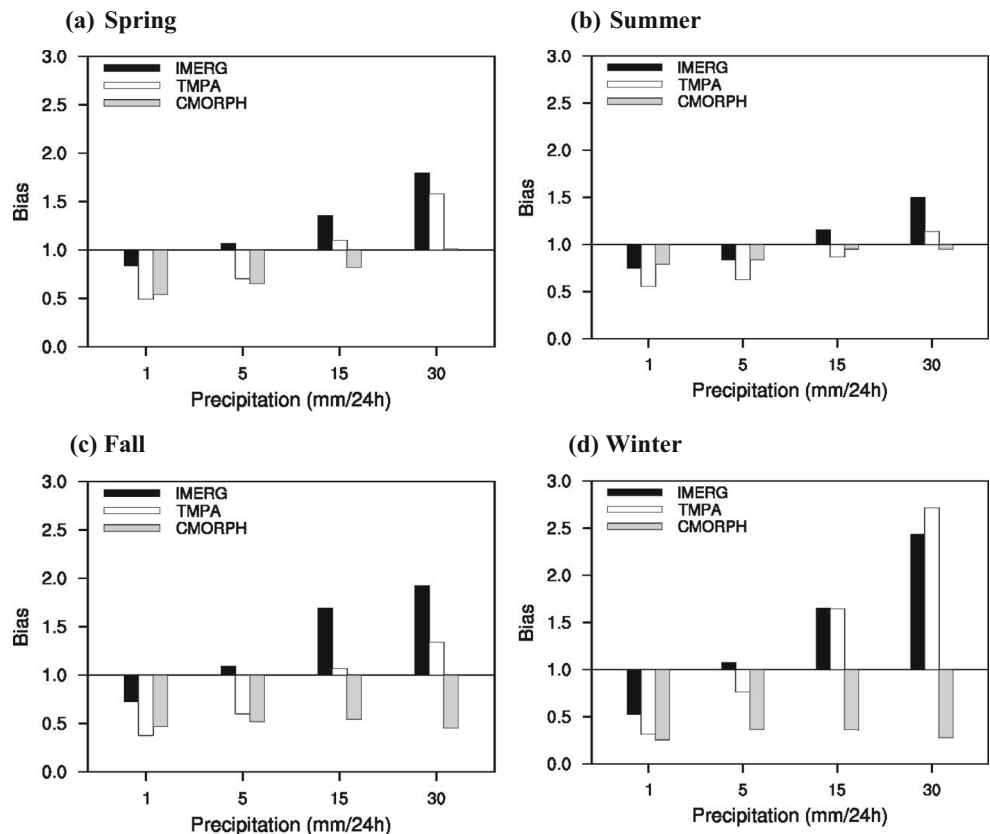


**Fig. 6** a Contingency table (2 × 2) and definition of performance measures for b frequency Bias index (Bias), c equitable threat score (ETS), e probability of detection (POD), f false alarm ratio (FAR), g success ratio (SR), and h critical success index (CSI)

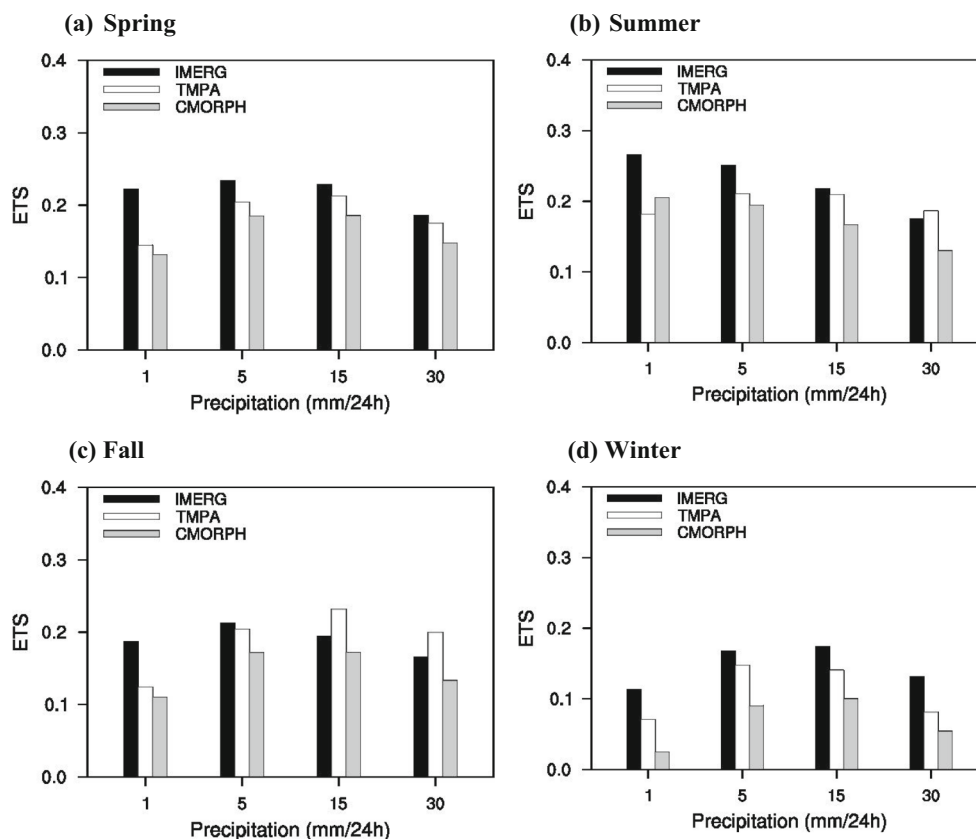
In order to summarize the performance of the three HRPPs, multiple measures of conditional detection are analyzed by using the visualizing method suggested by Roebber (2009), and this provides an easy method to compare the performance of different forecasts using various verification measures by representing several measures of forecast quality, such as POD, SR, CSI, and bias, in the same plot. The mathematical relationships used in visualizing the performance diagram are given in Fig. 6.

Figure 10 shows the seasonal performance diagrams for the three HRPPs verified against CPC gauge data. The general characteristics found in the performance of daily precipitation detection against CPC are as follows. All the diagrams exhibit a wide range of bias between 0.3 and 3.0 (dashed solid lines), and this varies depending on seasons and thresholds for each satellite product. Among them, the CMORPH (squares) shows overall underestimation (bias less than 1) for all seasons, and the performance appears to reduce further with high underestimation (especially in winter). In the case of IMERG and TMPA, they show underestimation for the lower threshold detection and overestimation for the larger threshold detection, thereby resulting in a high false alarm rate (FAR) to the higher precipitation thresholds (different colors indicate

**Fig. 7** Seasonal Bias index from IMERG, TMPA, and CMORPH product over East Asia against CPC unified gauge-based precipitation analysis for various daily precipitation thresholds corresponding to 1, 5, 15, and 30 mm day<sup>-1</sup>



**Fig. 8** Seasonal ETS from IMERG, TMPA, and CMORPH product over East Asia against CPC unified gauge-based precipitation analysis for various daily precipitation thresholds corresponding to 1, 5, 15, and 30 mm day<sup>-1</sup>



the precipitation thresholds). This implies that they tend to overestimate heavier precipitation but underestimate light precipitation. Nevertheless, there exist differences in the seasonal performance of precipitation detection. In the summer, all products show quite unbiased precipitation detection skills close to 1. They exhibit better performance since they are positioned toward the top-right portion of the diagram near the  $y = x$  line, thereby indicating a high POD and SR and near-unity bias (Fig. 10b). Conversely, winter leads to the lowest performance for the three HRPPs with a decreases in POD, CSI, and SR values for all thresholds (Fig. 10d).

In both summer and winter, the performance of IMERG (circles) appears superior to that of the others, showing a higher POD and CSI. In the spring and fall (Fig. 10a, c), the IMERG product (circle) has a relatively high POD (approximately 0.4) and CSI (0.18–0.32) when compared with that of the other products. The CMORPH shows a slightly larger discrepancy when compared with the other two products, thereby indicating a low POD and CSI with consistency in the underestimating characteristics.

In order to examine the gauge-based correction to the satellite products, we performed the same analysis by using the GPCC gauge observation but for a coarser

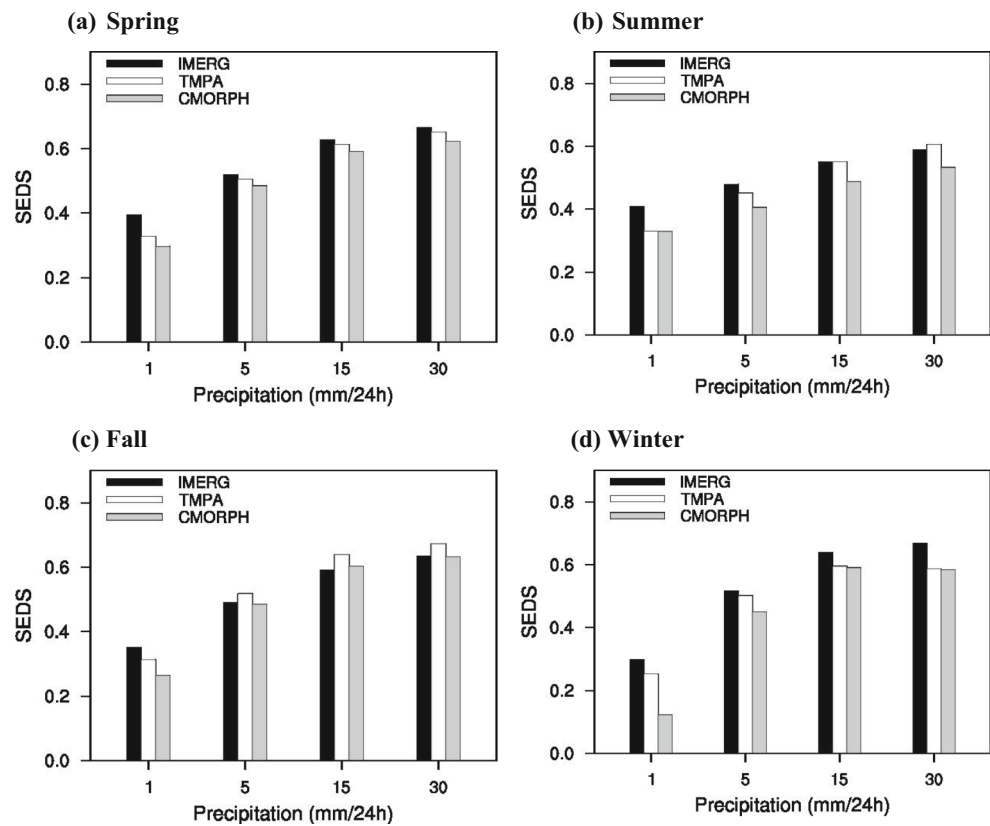
horizontal resolution of 1 degree, and the result is shown in Fig. 11. The bias characteristics of IMERG and TMPA are highly corrected when they are evaluated with GPCC, and this is more conspicuous in the spring and summer, while all satellite products still show significantly diverse bias results in winter. Nevertheless, IMERG exhibits the overall highest performance for all the threshold ranges. Additionally, the results of the performance diagram reinforce the findings presented in the preceding paragraph.

## 5 Summary and conclusion

In the study, the performance of the IMERG daily precipitation product is evaluated and compared with other HRPPs (TMPA and CMORPH) over the East Asian domain by using CPC gauge-based precipitation for a full year. The evaluation is conducted with respect to two aspects. First, spatial distributions of seasonal mean performance of the HRPPs are examined. Second, their accuracy with the different precipitation thresholds is verified via the contingency table method.

Spatial seasonal mean distributions of the three precipitation products exhibit overall agreement over land with

**Fig. 9** Seasonal SEDS from IMERG, TMPA, and CMORPH product over East Asia against CPC unified gauge-based precipitation analysis for various daily precipitation thresholds corresponding to 1, 5, 15, and 30 mm day<sup>-1</sup>



the exception of winter. Specifically, IMERG and TMPA display high similarity in seasonal mean bias and correlation of daily precipitation while the CMORPH tends to underestimate them. In winter, all products exhibit underestimated and uncorrelated winter precipitation for light precipitation over the northern Asian regions relative to CPC gauge precipitation. Among the three HRPPs daily precipitations, the IMERG product provides similar phase to CPC, with correlation coefficients above 0.7 over all seasons, but correlations with TMPA vary within a large range from 0.53 in winter to 0.75 in summer.

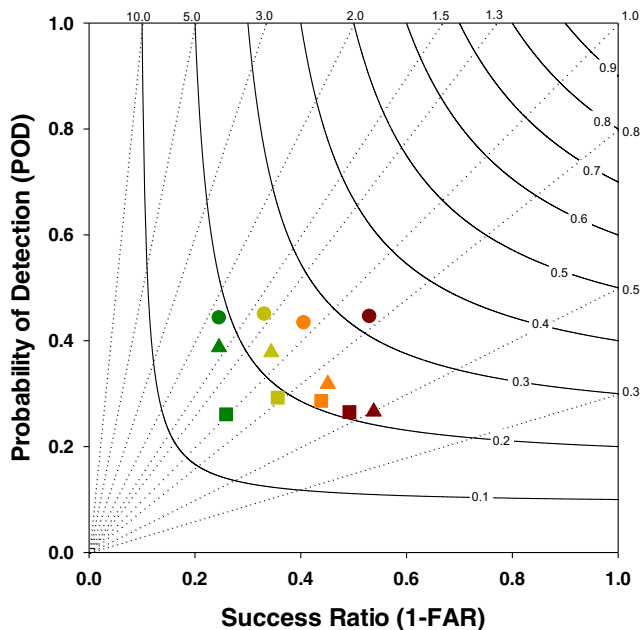
The accuracy of the three HRPPs is also measured based on precipitation detection verified against CPC gauge-based precipitation for various thresholds. The results indicate that the IMERG and TMPA precipitation products tend to underestimate with decreasing precipitation thresholds and overestimate with increasing the precipitation thresholds, while CMORPH exhibits persistent underestimation for all thresholds, which is more significant in winter. The TMPA and IMERG present similar performance characteristics exceeding those of CMORPH. The results indicate that IMERG reveals quite unbiased precipitation and a higher ETS when compared with those of the TMPA at a light precipitation threshold less than 5 mm day<sup>-1</sup>, but it also exhibits overestimated precipitation for the heavier precipitation threshold and a

slightly lower ETS when compared with the TMPA. However, the IMERG shows reliable performance in precipitation over East Asia for all seasons, showing higher POD, CSI, and SR.

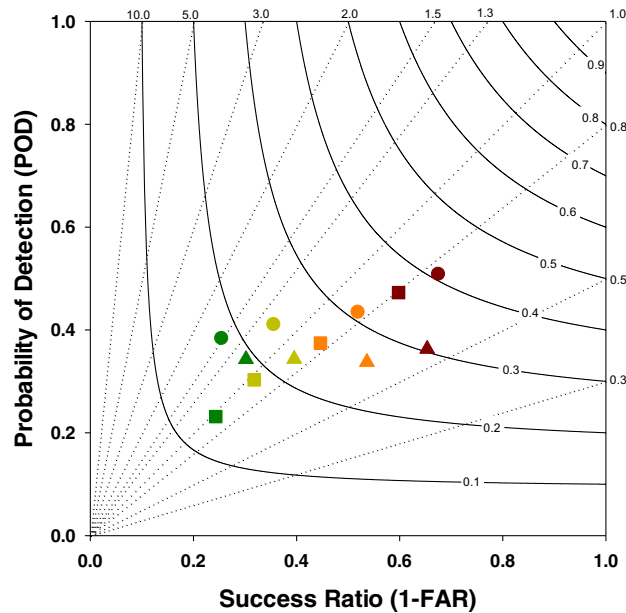
The impact of gauge-based bias correction on the satellite precipitation products is also investigated by evaluating HRPPs with GPCC gauge-based precipitation. The results reveal that bias correction using gauge observation is critical to final precipitation products, and thus the bias of TMPA and IMERG is significantly reduced and especially the spring and summer seasons. Nevertheless, the overall performance of IMERG and TMPA is comparable relative to both CPC and GPCC-daily.

In conclusion, performances of IMERG and TMPA are comparable with gauge-based precipitations but IMERG shows reliable performance in precipitation over East Asia against both CPC and GPCC gauge-based analysis precipitation. Overall underestimation and relatively low correlations are found from all products during winter when compared with that of gauge-based precipitations. It should be noted that winter precipitation accuracy as measured by ETS and SEDSs shows significant differences for all satellite products, and this is related to the relatively small data samples. However, it shows that the achievement of accurate winter precipitation amount is still challenging for satellite-based precipitation products, considering the diverse performance among

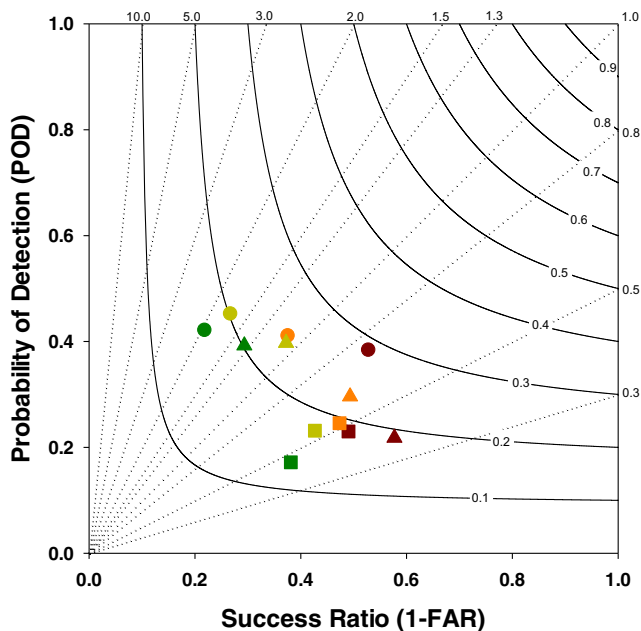
(a) Spring



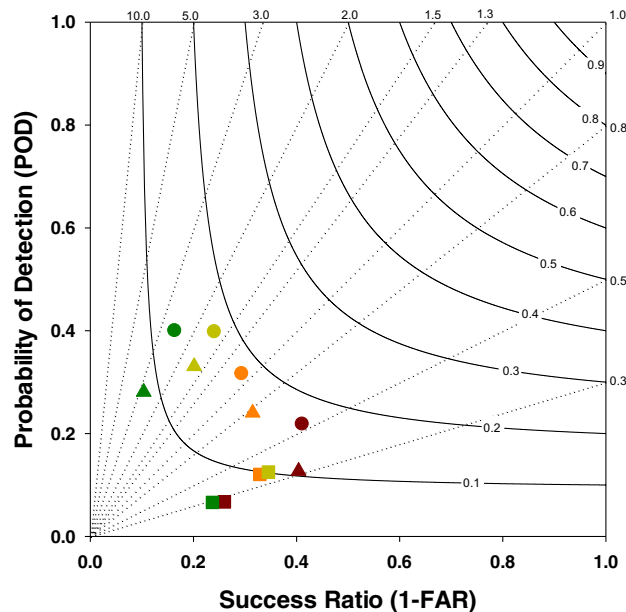
(b) Summer



(c) Fall



(d) Winter



Circle : IMERG / Triangle : TMPA / Square : CMORPH

Threshold (mm) 1.0 5.0 15.0 30.0

Fig. 10 Seasonal performance diagrams of IMERG (circle), TMPA (triangle), and CMORPH (square) daily precipitation against CPC for different thresholds of 1, 5, 15, and 30 mm day<sup>-1</sup> as depicted in different colors. The curved isolines denote CSI, dashed solid lines denote bias,

and POD and SR are given by the x- and y-axes (Optimal scores are in the upper right corner, and bias values close to 1 are typically considered optimal). Evaluation is performed on the same horizontal resolution with the reference ( $\times 0.5^\circ$ ) data

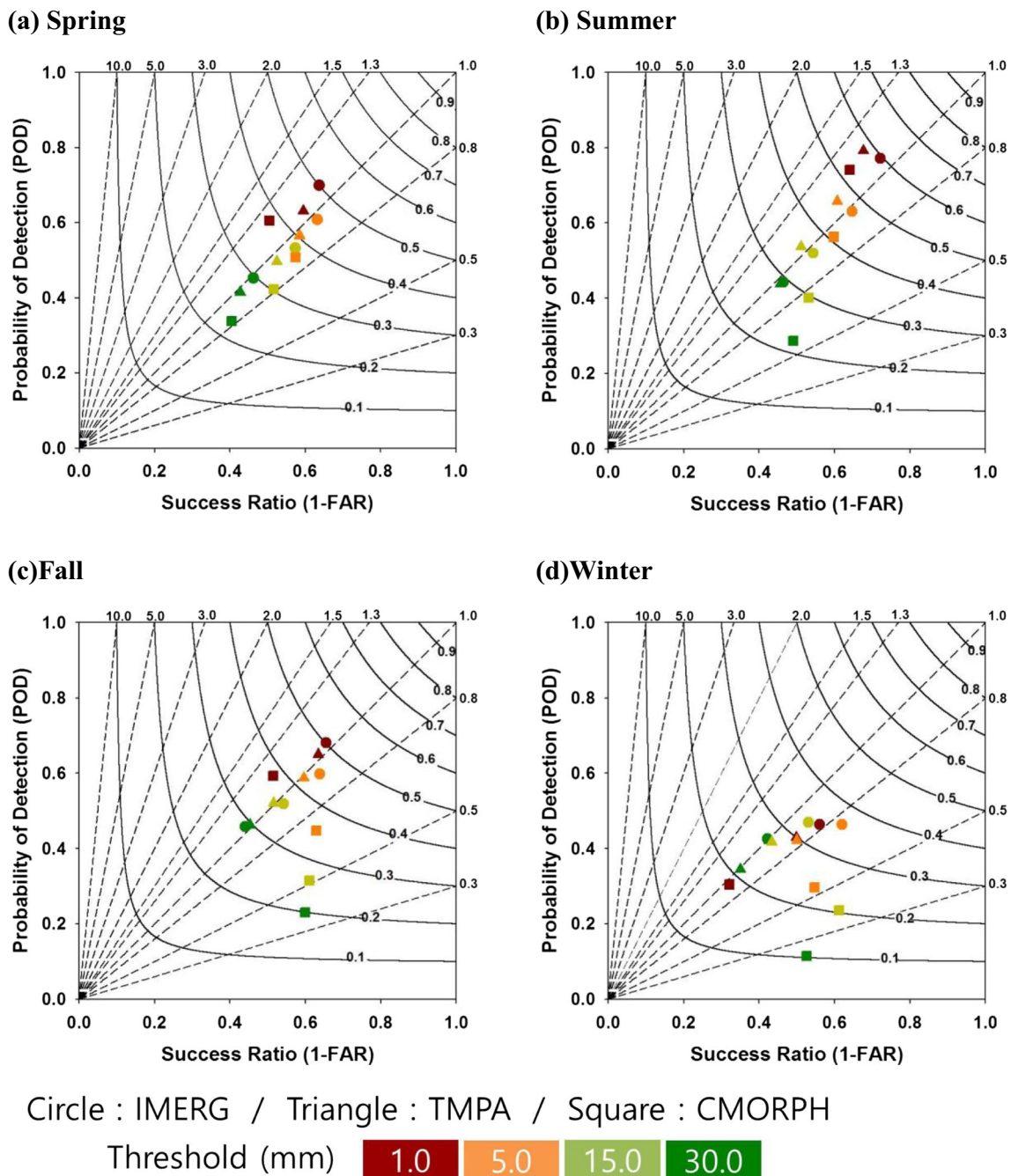


**Fig. 11** Seasonal performance diagrams of IMERG (circle), TMPA (triangle), and CMORPH (square) daily precipitation against relative to GPCP for different thresholds of 1, 5, 15, and 30 mm day<sup>-1</sup> as depicted in different colors. The curved isolines denote CSI, dashed solid lines denote

bias, and POD and SR are given by the  $x$ - and  $y$ -axes (Optimal scores are in the upper right corner; and bias values close to 1 are typically considered optimal). Evaluation is performed on the same horizontal resolution with the reference ( $\times 1.0^\circ$ ) data

products in terms of both spatial distributions and conditional verification scores for the winter season.

The period in which IMERG data is available, remains limited, and thus it is slightly early to draw a definite conclusion. Nevertheless, the results of the assessment study indicate the validity of the IMERG product, and thus HRPP users can use it to estimate not only seasonal precipitation but also daily

precipitation, which can be potentially used as reference precipitation data to validate NWP models.

**Acknowledgments** This work has been carried out through the R&D project on the development of global numerical weather prediction systems of Korea Institute of Atmospheric Prediction Systems (KIAPS) funded by Korea Meteorological Administration (KMA).

**Publisher's note** Springer Nature remains neutral with regard to jurisdictional claims in published maps and institutional affiliations.

## References

- Adler CK, Petty G, Morissey M, Goodman HM (2001) Intercomparison of global precipitation products: the third Precipitation Intercomparison Project (PIP-3). *Bull Am Meteorol Soc* 82:1377–1396
- Aonashi K et al (2009) GSMaP passive, microwave precipitation retrieval algorithm: algorithm description and validation. *J Meteorol Soc Japan* 87A:119–136
- Arkin PA, Xie PP (1994) The global precipitation climatology project: first algorithm Intercomparison project. *Bull Am Meteorol Soc* 75: 401–419
- Barrett EC et al (1994) The first WetNet precipitation intercomparison project: interpretation of results. *Remote Sens Rev* 11:303–373
- Behrangi A, Hsu K-L, Imam B, Sorooshian S, Huffman GJ, Kuligowski RJ (2009) PERSIANN-MSA: a precipitation estimation method from satellite-based multispectral analysis. *J Hydrometeorol* 10: 1414–1429
- Chen M, Shi W, Xie P, Silva VBS, Kousky VE, Higgins RW, Janowiak JE (2008) Assessing objective techniques for gauge-based analyses of global daily precipitation. *J Geophys Res* 113. <https://doi.org/10.1029/2007JD009132>
- Dodge J, Goodman HM (1994) The WetNet project. *Remote Sens Rev* 11:5–21
- Ebert EE, Manton MJ (1998) Performance of satellite rainfall estimation algorithms during TOGA COARE. *J Atmos Sci* 55:537–1557
- Ebert EE, Manton MJ, Arkin PA, Allam RJ, Holpin CE, Gruber A (1996) Results from the GPCP Algorithms Intercomparison Program. *Bull Am Meteorol Soc* 77:2875–2887
- Hogan RJ, O'Connor EJ, Illingworth AJ (2009) Verification of cloud-fraction forecasts. *Q J R Meteorol Soc* 135:1494–1511
- Hou AY et al (2014) The global precipitation measurement mission. *Bull Am Meteorol Soc* 95:201–722
- Huffman GJ, Adler RF, Bolvin DT, Gu G, Nelkin EJ, Bowman KP, Hone Y, Stocker EF, Wolff DB (2007) The TRMM multisatellite precipitation analysis (TMPA): quasi-global, multiyear combined-sensor precipitation estimates at fine scales. *J Hydrometeorol* 8:38–55
- Huffman GJ, Adler RF, Bolvin DT, Gu G, Nelkin EJ (2010) The TRMM multi-satellite precipitation analysis (TMPA). In Hossain F and Gebremichael M (Eds.) *Satellite rainfall applications for surface hydrology*. Springer, Dordrecht. [https://doi.org/10.1007/978-90-481-2915-7\\_1](https://doi.org/10.1007/978-90-481-2915-7_1)
- Huffman GJ, Bolvin DT, Braithwaite D, Ksu K, Joyce R, Kidd C, Nelkin EJ, Xie P (2015a) NASA Global Precipitation Measurement (GPM) Integrated Multi-satellite Retrievals for GPM (IMERG). Algorithm Theoretical Basis Doc., version 4.5, 26 pp
- Huffman GJ, Bolvin DT, Nelkin EJ (2015b) Integrated Multi-satellite Retrievals for GPM (IMERG) technical documentation. NASA Doc, 47 pp
- Huffman GJ, Bolvin DT, Nelkin EJ (2015c) Day 1 IMERG final run release notes. NASA Doc., 9 pp
- Janowiak JE, Joyce RJ, Yarosh Y (2001) A real-time global half-hourly pixel-resolution infrared dataset and its applications. *Bull Am Meteorol Soc* 82:205–217
- Joyce RJ, Xie P (2011) Kalman filter-based CMORPH. *J Hydrometeorol* 12:1547–1563
- Joyce RJ, Janowiak JE, Arkin PA, Xie P (2004) CMORPH: a method that produces global precipitation estimates from passive microwave and infrared data at high spatial and temporal resolution. *J Hydrometeorol* 5:487–503
- Kim K, Park J, Paik J, Choi M (2017) Evaluation of topographical and seasonal feature using GPM IMERG and TRMM 3B42 over Far-East Asia. *Atmos Res* 187:95–105
- Lee J, Lee E-H (2018) Evaluation of daily precipitation estimate from integrated Multisatellite Retrievals for GPM (IMERG) data over South Korea and East Asia. *Atmosphere* 28(3):273–289 (in Korean with English abstract)
- Liu Z (2016) Comparison of Integrated Multisatellite Retrievals for GPM (IMERG) and TRMM Multisatellite Precipitation Analysis (TMPA) monthly precipitation products: initial results. *J Hydrometeorol* 17: 777–790
- Prakash S, Mitra AK, Pai DS, Aghakouchak A (2016) From TRMM to GPM: how well can heavy rainfall be detected from space? *Adv Water Resour* 88:1–7
- Roebber PJ (2009) Visualizing multiple measures of forecast quality. *Wea Forecasting* 24:601–608
- Schneider U, Becker A, Meyer-Christoffer A, Ziese M, Rudolf B (2011) Global precipitation analysis products of the GPCC. GPCC doc., DWD, 13 pp. [Available online at [ftp://ftp.dwd.de/pub/data/gpcc/PDF/GPCC\\_intro\\_products\\_v2011.pdf](ftp://ftp.dwd.de/pub/data/gpcc/PDF/GPCC_intro_products_v2011.pdf)]. Accessed Jan 2017
- Smith EA et al (1998) Results of the WetNet PIP-2 project. *J Atmos Sci* 55:1483–1536
- Sorooshian S, Hsu K-L, Gao X, Gupta HV, Imam B, Braithwaite D (2000) Evaluation of PERSIANN system satellite-based estimates of tropical rainfall. *Bull Am Meteorol Soc* 81:2035–2046
- Sun Q, Miao C, Duan Q, Ashouri H, Sorooshian S, Hsu K-L (2018) A review of global precipitation data sets: data sources, estimation, and intercomparisons. *Rev Geophys* 56:79–107. <https://doi.org/10.1002/2017RG000574>
- Xie P, Yatagai A, Chen M, Hayasaka T, Fukushima Y, Liu C, Yang S (2007) A gauge-based analysis of daily precipitation over East Asia. *J Hydrometeorol* 8:607–626